Published in final edited form as:
Exp Eye Res. 2014 December ; 129: 107–118. doi:10.1016/j.exer.2014.10.018.

Retinal Vasculature of Adult Zebrafish: *In Vivo* Imaging Using Confocal Scanning Laser Ophthalmoscopy

Brent A. Bell[1], **Jing Xie**[1], **Alex Yuan**[1,2], **Charles Kaul**[1], **Joe G. Hollyfield**[1,2], and **Bela Anand-Apte**[1,2]

[1]Department of Ophthalmic Research, Cole Eye Institute, Cleveland Clinic, Cleveland, OH

[2]Department of Ophthalmology, Cleveland Clinic Lerner College of Medicine of Case Western Reserve University, Cleveland, OH

Abstract

Over the past 3 decades the zebrafish (*Danio rerio*) has become an important biomedical research species. As their use continues to grow additional techniques and tools will be required to keep pace with ongoing research using this species. In this paper we describe a novel method for *in vivo* imaging of the retinal vasculature in adult animals using a commercially available confocal scanning laser ophthalmoscope (SLO). With this instrumentation, we demonstrate the ability to distinguish diverse vascular phenotypes in different transgenic GFP lines. In addition this technology allows repeated visualization of the vasculature in individual zebrafish over time to document vascular leakage progression and recovery induced by intraocular delivery of proteins that induce vascular permeability. SLO of the retinal vasculature was found to be highly informative, providing images of high contrast and resolution that were capable of resolving individual vascular endothelial cells. Finally, the procedures required to acquire SLO images from zebrafish are non-invasive, simple to perform and can be achieved with low animal mortality, allowing repeated imaging of individual fish.

Keywords

zebrafish; confocal; SLO; imaging; retina; scanning laser ophthalmoscope; blood retinal barrier

1. Introduction

The zebrafish, (*Danio rerio*), has become a popular experimental animal for basic research (Bilotta and Saszik, 2001; Hughes, 2013). The number of publications using this species has grown over the past three decades with over 20,000 publications currently available online. Although the use of rodents is still more prevalent (Hughes, 2013), a PUBMED search by

Corresponding Author: Brent A. Bell, Cole Eye Institute, 9500 Euclid Ave./i31, Cleveland, Ohio 44195; Phone: (216) 445-5832; bellb3@ccf.org.

our group revealed that publications using zebrafish are currently outpacing those using mice, rats and Drosophila (unpublished data). If this rate continues, the number of zebrafish publications could potentially eclipse those of Drosophila and rodents in the future.

Zebrafish offer a number of advantages that make them more convenient and less expensive to use in research than other vertebrates. They are easy to breed (Kari et al., 2007), and much less expensive to maintain than rodents (Vogel and Weinstein, 2000); they reach maturity within 3 months and are easily manipulated for production of transgenic and mutant strains; and as a vertebrate, 70% of human genes have at least one ortholog in zebrafish (Howe et al., 2013). The animal is robust and easily manipulated considering its small size and unique aquatic environmental requirements.

Zebrafish are substantially smaller than mice and the ocular system is proportionally smaller as well. The dimensions of adult zebrafish pupil and lens are approximately 1 mm in diameter (Dahm et al., 2007; Farkas et al., 2010) making imaging of the fundus through the pupil rather challenging. New approaches have recently emerged for imaging ocular tissues from both adult and embryonic zebrafish. To date fish have been successfully imaged *in vivo* with confocal SLO (Farkas et al., 2010), fundus imaging (Duval et al., 2013; Tschopp et al., 2010), OCT (Bailey et al., 2012; Kagemann et al., 2008; Podoleanu et al., 2008; Rao et al., 2006) and traditional confocal microscopy (Watanabe et al., 2010). Extraocular confocal imaging of the zebrafish eye has been described in embryos for vascular angiography (Weinstein et al., 1995) and retinal cell morphology (Watanabe et al., 2010). Whole embryo OCT imaging has also been used to follow the development of ocular structures (Kagemann et al., 2008). To our knowledge, this is the first report describing the use of a commercially available clinical instrument to acquire SLO images from the adult zebrafish eye in a transpupillary manner.

Scanning laser ophthalmoscopy (SLO), first reported by (Webb et al., 1987), is now a well-established clinical imaging technique in ophthalmology (Hassenstein and Meyer, 2009). The clinical instrument has also found wide use in non-clinical research for imaging eyes in small animal models (Hossain et al., 1998; Seeliger et al., 2005). SLO is capable of visualizing endogenous features of the retina as well as exogenous signal from fluorophores injected into the systemic circulation as they enter retinal vessels (Seeliger et al., 2005), protein labels for visualization of photoreceptors (Beck et al., 2010; Seeliger et al., 2005), inflammatory monocytes (Paques et al., 2006), and apoptotic cells (Maass et al., 2007). Building on these previous examples in other research animals, we decided to investigate the feasibility of imaging retinal vessels in zebrafish using a commercially available SLO. This paper describes in detail our experience with SLO in transpupillary imaging of retinal vasculature and provides examples of images that can be routinely obtained from anesthetized adult zebrafish.

2.0 Materials and Supplies

2.1 Animal Models and Care

All manipulations conformed to the ARVO Statement for Care and Use of Animals in Ophthalmic and Visual research. The Cleveland Clinic Institutional Animal Care and Use

Committee approved all experimental procedures and manipulations.. Adult zebrafish used were maintained at 28.5°C on a 14-hour light/10-hour dark cycle according to standard procedures (Westerfield, 2007). Fish, 3 – 15 months old were used for the studies described. Zebrafish lines examined by SLO imaging included *Tg(flk1:EGFP)*(Jin et al., 2005), Tg(flk1:mCherry), Tg(flk1:nGFP), Tg(l-fabp:DBP-EGFP) (Xie et al., 2010) and *Tg(apoeb:lynEGFP)zf147* (Matthews and Varga, 2012; Peri and Nusslein-Volhard, 2008). In the *Tg(flk1:EGFP) and Tg(flk1:mCherry)* models, EGFP and RFP (mCherry) are expressed in the cytoplasm of vascular endothelial cells while *Tg(flk1:nGFP)* zebrafish express GFP in the nuclei of vascular endothelial cells. In the *Tg(l-fabp:DBP-EGFP)* model, the fluorescent vitamin D binding protein (DBP) is fused with EGFP. DBP is a member of the albumin gene family and found in plasma. DBP-EGFP fusion protein is synthesized by hepatocytes and secreted into the blood plasma compartment. *Tg(apoeb:lynEGFP)zf147* zebrafish express EGFP in Müller glia of the neural retina.

2.2 SLO Instrumentation

Retinal imaging was performed using a Heidelberg Retina Angiograph 2 (HRA2) SLO, which is the predecessor to the Spectralis® family of ophthalmic imaging instruments currently available from Heidelberg Engineering USA, Inc (Carlsbad, CA). The HRA2 has two primary settings, known as “R” and “A”, which refer to reflectance and angiography modes of operation, respectively. A lever on the scan head allows alternation between these two modes of operation. Within these modes are several additional imaging channels that can be deployed using various combinations of illumination and/or acquisition parameters. Each channel is uniquely independent and permits probing with specific illumination and/or excitation wavelength parameters. As a result, this instrument can be used to non-invasively monitor tissue changes over time using 5 separate channels, with each channel providing unique information about the tissue being examined. The various modes and sub-mode channels are shown in Table 1.

With the instrument in “R” mode, reflectance images are collected via two channels that are referred to as Red Free-Dark Field (RFDF) and Infrared-Dark Field (IRDF), respectively. Red Free and Infrared refers to laser illumination wavelengths of 488 and 815 nm, respectively. The term “dark field” refers to images that are collected using crossed (i.e. orthogonal) polarization filters in the illumination and signal detection arms of the instrument. As the instrument scans the retina, a two-dimensional fundus image is generated from the reflected signal collected in retro-fashion. The visual contrast observed in dark field images originates predominantly from the birefringent properties of the tissue (Heidelberg Engineering, 2006, 2008).

In “A” or angiography mode, the instrument is capable of collecting both autofluorescence and reflection data, in addition to typical endogenous and exogenous fluorescence signals from injected fluorophores as well as GFP signals (Paques et al., 2006). This mode permits image collection from 3 separate channels, each with excitation/illumination wavelengths centered at 488 or 790nm. The three channels are referred to as FA, ICGA, and IR, which correspond to Sodium Fluorescein Angiography, Indocyanine Green Angiography and Infrared reflectance, respectively. Used in the absence of exogenous fluorophores (i.e. NaF,

ICG, or GFP), FA and ICGA channels are often referred to by different nomenclature, which are AF (blue/green autofluorescence @ 488 excitation) and IRAF (infrared autofluorescence @ 790nm excitation). For quality control, SLO excitation and illumination laser intensities are periodically measured using a calibrated Nova optical power/energy readout unit (Ophir-Spiricon LLC, N. Logan, UT) and optical power detection head (PD300-3W).

All images were collected using the wide-field objective lens (55°). For single frame images the system was operated in high-resolution mode, which provided nominal field of view options of 55° (~ 1.9 MP), 35° (~1 MP), and 25° (~0.59 MP) with acquisition rates of 5, 7 and 9 frames/sec, respectively. Dynamic imaging (i.e. movies) was performed with the system set at high-speed mode, which provides nominal field of view options of 55° (0.46 MP), 35° (0.26 MP), and 25° (0.15 MP) with acquisition rates of 9, 13, and 16 frames/sec, respectively. The HRA2 system was operated under Heidelberg Eye Explorer software v1.7. Online algorithms within the HRA2 control software enable automatic real-time averaging and tracking (ART) of sequentially collected images. This parameter was preset for 25 frame averaging to further enhance image contrast and resolution with all imaging sub-modes. A manual, z-axis, focus adjustment (Range −20 to 200 D) on the system permits linear adjustment of the SLO confocal axial imaging plane within the ocular tissue. The adjustable focus feature was used extensively to identify and document vasculature features observed in the various zebrafish models investigated.

In order to better facilitate imaging of a small animal model, we removed the head/chin rest from our instrument that is provided for clinical use and replaced it with a mounting stage designed for animal use (Heidelberg Engineering USA).

2.3 Image Processing, Data Analysis, and Statistical Analysis

2.3.1 General Information on the Acquisition, Exporting and Display of Images

—All images were collected with the automatic normalization and brightness features inactivated in the HRA2 acquisition software. Single and composite images were exported as uncompressed, 8-bit TIFF files. Dynamic recordings were exported as uncompressed AVI files. ImageJ (v1.47b) software (Rasband) was used to open exported files for post-collection processing and analysis. By default, the images open (*File>Open*) as RGB color files in ImageJ and were converted to 8-bit grayscale images (*Image>Type>8-bit*). Scale bars displayed in the exported images, which are calibrated for human ocular dimensions and not zebrafish, were removed [*Color Picker (R, G, B values = 0, 0, 0)* & *Pencil Tools (size 20)*] from the lower left corner. ImageJ was used to enhance brightness and/or contrast (*Image>Adjust>Brightness/Contrast>Auto*) as well as pseudocolor (*Image>Lookup Tables>Green*) some angiography images post-acquisition to better accentuate GFP, EGFP or RFP fluorescence. This was performed strictly on representative images intended for display in the manuscript (Figs. 1C–E, J–L) so that minute detail could be visualized. In contrast, all quantitative analysis (Table 2 and Figs. 2–4) were performed on unaltered TIFF images. No corrections or adjustments to signal intensity and/or contrast were made prior to performing avascular space area and background intensity level measurements.

2.3.2 Vascular Anatomy and Background Amplitude Comparisons between Zebrafish and Mice—Images from *Tg(l-fabp:DBP-EGFP)* zebrafish and mice injected with NaF were obtained to compare retinal vasculature anatomy between species. The description of SLO and/or fundus imaging using NaF for mouse vasculature has been previously published (Paques et al., 2006; Seeliger et al., 2005). This technique is used frequently in rodents *in vivo* to assess vascular leakage from retinal vessels (Xia et al., 2008) and laser-induced choroidal neovascularization (CNV) *in vivo* (Balaggan et al., 2006; Luhmann et al., 2009). Briefly, for our studies, mice were injected with 10 μl of 1% NaF intraperitoneally (IP) and imaged 4 minutes later using FA mode. Images of the deep and superficial vascular plexus, described by Paques et al (Paques et al., 2006;), were obtained by adjusting the SLO scan focus and using ART and 25 frames averaging.

Extravascular Space Mean Intensity (ESMI) and Area (ESMA) from both species were measured using the following image processing steps in ImageJ. Images were exported, opened and converted to grayscale images as aforementioned in 2.3.1. Afterwards an automated threshold function (*Image>Adjust>Threshold>Auto with the following selections* "*Yen* & *Red*"*>Apply*) in ImageJ, which we have abbreviated as "YAT", was applied to isolate the avascular space for analysis. After running the function, the retinal vasculature is preserved in grayscale and the image window frame (i.e. black mask surrounding the circular SLO FOV) and extravascular spaces become highlighted in red. To further isolate the ROI (circular FOV region) from the image frame mask, the lower limit arrow tab in the ImageJ Threshold function window must be changed from "0" to "1". This step changes the image mask from red back to black and fully isolates the avascular space from the vasculature and image frame mask.

Next, immediately prior to collecting the area and intensity measurements, the image scale was set to default in pixels (*Analyze>Set Scale>*"*Click to Remove Scale*") and the "Area", "Mean", "Area Fraction" and "Limit to Threshold" boxes were selected within the "Set Measurements" window (*Analysis>Set Measurements> select* "*Area*", "*Mean*", "*Area Fraction*" *and* "*Limit to Threshold*"). The ESMI and ESMA were then obtained using the measure function (*Analyze>Measure>Results*).

2.3.3 Quantification of Vascular Leakage Following Intraocular Injections—A procedure was developed to measure and quantify signal changes from the avascular space of *Tg(l-fabp:DBP-EGFP)* zebrafish following intraocular injections (IOI). For these experiments, FA images were acquired with a camera sensitivity (i.e. gain) setting of 70 from a possible range of 31-107. In the majority of fish (>80%) at baseline, optimal images could be obtained using this setting without evidence of image pixel saturation, which coincidently, occurs at a grayscale level of 251 and is revealed to the operator by colored pixels on the display screen (Charbel Issa et al., 2012). If saturation was observed, either from avascular leakage or from the bright, EGFP laden vessels (most notably from the vascular trunk region), a series of additional images (3 minimum, but up to 6 if saturation was still observed at lower sensitivities) were collected using lower sensitivity settings taken at half-decade increments (i.e. 65, 60, 55, 50, etc.). Images (e.g. 70 only if unsaturated) and/or image sequences (e.g. 70, 65, 60 and so on if saturation was noted) were then exported to ImageJ as aforementioned in 2.3.1 and were analyzed using the YAT function

described in 2.3.2. For animals without saturated images the analysis was straightforward and identical to that described in 2.3.2. Animals with saturated images at a sensitivity setting of 70 underwent a correction process developed to address the 8-bit dynamic range limitation of the SLO detection system. The sensitivity of the HRA2 and Spectralis family of instruments has been previously reported to have an exponential change in signal gain relative to the linear change (31-107) in sensitivity setting via the console selection dial (Delori et al., 2011). Knowing this information we were able to devise a correction process for analyzing saturated images from animals that had more fluorescence yield at baseline or any other time point (e.g. from EGFP expression yield and/or size/volume of vascular head which typically happens to be the brightest object in an image) or exhibited an exceptional amount of leakage signal that exceeded the 8-bit dynamic range of the HRA2 camera at a sensitivity setting of 70. With these particular animals, each additional sub half-decade image was opened in ImageJ, converted to grayscale, and then double-checked for evidence of pixel saturation using the Histogram function (*Analyze>Histogram*). The first non-saturated image identified (e.g. say 65 for example), and the two following lower sub half-decade intensities (e.g. 60 & 55) had the YAT function applied to them to obtain the ESMI. Mean pixel signal amplitudes from the unsaturated, tri-image sequence (e.g. 65-60-55) were then plotted in MS excel. In excel these data points were fitted with an exponential curve to obtain the fit parameters (i.e. equation constants). The equation was then used to extrapolate the mean extravascular signal value at a sensitivity setting of 70.

2.3.4. Procedure Times—Zebrafish preparation and imaging times were obtained from a group of 35 animals and displayed as Mean ± S.D.

2.3.5 Statistical Analysis—Data were plotted and analyzed for statistical significance in Graphpad Prism v6 using ordinary one-way ANOVA and multiple t-test. P-values of ≤0.05 were considered significant. In figures and tables, P-values are denoted using asterisks as follows: *P≤ 0.05, **P≤ 0.01, ***P≤ 0.001, ****P≤ 0.0001.

3.0 Detailed Methods

3.1 Zebrafish Sedation

Fish were individually anesthetized using ethyl 3-aminobenzoate methanesulfonic acid salt (Product #118000500, Acros Organics, Morris Plains, NJ), also known as “MS-222” or “tricaine”, as previously described (Matthews and Varga, 2012). We found it convenient to make Tricaine stock solution (100 ml) in bulk, aliquot it into smaller volumes (10 ml), stored at −20°C, and thaw as needed on a weekly basis. Tricaine stock solutions (4% w/v) were made by combining 97.9ml of double distilled water with 2.1 ml of 1 M Trizma base (Sigma Life Sciences T1503-1KG, MW: 121.14 g/mol) (12.114 g/100 ml H_2O) and 400 mg Tricaine powder. After thawing, stock solutions can be refrigerated at 4°C between uses for up to 5 days. Immediately before use, a “starter” Tricaine anesthetic solution was prepared by adding 2 ml of the 4% Tricaine stock to 100 ml of clean fish tank water. Fish were then placed in the anesthesia solution contained in a 250 ml glass beaker and closely monitored for several minutes for changes in swimming behavior, righting reflex and gill plate movement. Fish were considered ready for imaging when they showed no evidence of

movement and did not respond to touch or handling. In our experience, ~3 ml of Tricaine stock added to 100ml of tank water (~0.12% or 0.120 mg/ml) is sufficient to induce short term anesthesia, however, we have successfully employed Tricaine doses ranging from 0.120 to 0.170 mg/ml.

3.2 Intraocular Injections

For vascular leakage experiments, zebrafish were anesthetized with Tricaine and intraocular injected (IOI) through the superior-nasal sclera using a pulled glass capillary pipette (30 μm diameter) and syringe pump (PV830 Pneumatic Picopump, World Precision Instruments, Sarasota, FL). In the first experiment, 0.8 μl (20 ng) of Bovine Serum Albumin (BSA) (Product# A7030, Sigma-Aldrich) reconstituted in phosphate buffered saline (PBS) containing 0.005% NaF was administered once to the right eye 24 hours after baseline imaging. In a second experiment, 0.8 μl (20 ng) of BSA in PBS was administered once to the right eye 24 hours after baseline imaging. A second group of animals was imaged daily and served as non-injected controls. In a third experiment, 0.8 μl of three different concentrations (20, 40, & 80 ng) of Bradykinin (BDK, Catalog #3004, TOCRIS Bioscience, Minneapolis, MN) reconstituted in PBS was administered once to the right eye 24 hours after baseline imaging. For an injection control, 0.8 μl (20 ng) of BSA in PBS was administered once to the right eye in a separate group of animals.

3.3 Pre-imaging Preparation

Once immobilized, which took on average 311 +/− 127 seconds, fish were removed from the 250 ml beaker using a plastic ladel and placed on a customized holder. The holder dimensions are 1.3 cm (W) × 3.5 cm (L) × 1 cm (H) constructed from a silicone finger mat (Item #1502E, Ambler Surgical, Exton, PA). The silicone fingers (i.e. vertical posts) enable positioning of the fish in the normal swimming orientation (Fig. 1A). The right eye was lightly touched with the tip of a cellulose sponge (Keraspear, Medtronic Xomed, Inc. Jacksonville, FL) to remove excess water from the cornea. The PMMA contact lens (Ø=5.2mm, r = 2.7mm, center thickness = 0.4mm, Cantor & Nissell, Ltd., Northamptonshire, U.K.) was picked up with small curved forceps and a single drop (~20ml) of Systane® Ultra hydrating tears (Alcon Laboratories, Ft. Worth, TX) was applied to the concave surface. The contact lens was then placed on the eye and manually held in position for a moment (~3 s) until adherent via surface tension. The process of removing the fish from the anesthesia solution, position in the holder and applying the contact lens can be accomplished in approximately 30 seconds.

3.4 Transpupillary SLO Imaging

The holder containing the fish with applied contact lens is then moved to the SLO imaging platform (Fig. 1B), (CL2 Table Clamp, Thorlabs, Inc., Newton, NJ) and held in place with double-stick tape (3M, St. Paul, MN). The holder is attached to an adjustable camera ball mount (SLIK model SBH-320, THK Photo Products, Huntington Beach, CA) in order to align the eye for imaging. Imaging of the right eye only requires 198 +/− 59 seconds and will vary depending on the number of images collected.

Imaging of inner retina, including the surface retinal vasculature and nerve fiber layer, is best accomplished with an internal myopic lens (−12 Diopter) correction set via the HRA2 control panel. This setting adds some divergence to the normally collimated SLO laser beam emerging from the instrument and when focused by the cornea and lens, extends the laser focus plane further into the ocular tissue. Extending the focusing depth enables one to reach the plane of interest (i.e. retinal vessels) by changing the focus adjustment knob on the SLO scan head. Performing this focusing exercise on each fish ensures that the best image plane is identified.

To acquire images immediately post-injection (IPI), additional myopic corrections are necessary to visualize the vascular plexus, which is displaced and/or distorted by the IOI. This adjustment extends the scanning laser focal plane further into the retina. This requires an atypical change to the myopic lens position in the SLO scan head via an engineering service mode diagnostics window (Note: Should one have hesitation regarding this simple change they should contact Heidelberg Engineering Technical Support for guidance). Briefly, to perform this adjustment, it is necessary to have the HRA2 system running with a live imaging window open and actively scanning. It is best to do this well before a fish is ready to be imaged as this routine can take up to a minute to perform. Depress the following keys (CTRL>ALT>SHFT>D) on the keyboard to open the service window. The Z module adjustment is located in the upper right hand corner of this window. The typical home position of the Z module is ~260 and it will need to be reduced to a value that can range from 150–240 using the “<<” and “<” selections. (Note: Care should be taken when venturing beyond a setting of “0” as the translation stage that advances the myopic lens assembly may get stuck and not retract with the usual commands. Should this happen it is necessary to contact Heidelberg Engineering Technical Support for assistance to rectify the issue.)

For reference, the Z module home positions specific on our HRA2 for 0 D (i.e. emmetropic) and −12 D (myopic) are “261” and “240”, respectively. Once the Z module parameter has been changed to the desired location the service mode window can be closed. The HRA2 system should retain this configuration throughout the duration of the imaging session until the instrument is turned off or reset by the user in the service window. This modification adds a substantial amount of additional myopic correction (−150 D or more) that should now enable visualization of retinal vasculature IPI.

Fig. 1C–E, J shows representative fluorescence images of retinal vasculature in Tg(flk1:EGFP), Tg(flk1:mCherry), Tg(flk1:nGFP), and Tg(l-fabp:DBP-EGFP) zebrafish models. Fig. 1C and 1D show GFP and RFP expression in endothelial cell cytoplasm of *Tg(flk1:EGFP)* and *Tg(flk1:mCherry*) lines, respectively. The mCherry signal is weaker relative to the GFP since 488nm is not the optimal wavelength to employ for excitation of RFP. Fig. 1E shows EGFP expression in endothelial nuclei of retinal vasculature in *Tg(flk1:nGFP)* zebrafish. Note that distinct, individual, fluorescent protein expressing nuclei are easily resolved in Fig. 1E and that the reporter morphology is distinct from the lines expressing either GFP or RFP in the cytoplasm (Fig. 1C or 1D).

Appreciable native signal contrast was also observed at the vitreoretinal interface using IR imaging mode (see Supplemental Video 1). At this interface, retinal vessels and nerve fibers could be imaged emanating from the optic disc. IRDF and RFDF modes were also capable of visualizing these features (images not shown). Measuring the optic nerve diameter (~200 μm) from radial cryostat sections suggests that the SLO image FOV is ~1 mm (data not shown).

Autofluorescence mode (AF or FA) was useful for visualizing and investigating the retinal vasculature with either intraperitoneally injected NaF (Fig. 1F–I) or by imaging the *Tg(l-fabp:DBP-EGFP)* model which has endogenous GFP-DBP (Fig. 1J) circulating throughout the vascular compartment. Fig. 1F–I is an example of the traditional method used for performing angiography in a small animal where the contrast agent (i.e. NaF) is injected via a readily accessible vein (i.e. tail vein of the mouse), or alternatively, into the intraperitoneal (IP) cavity. Fig. 1F–I shows a *Tg(apoeb:lynEGFP)zf147* or “GFP-ApoE” fish that has undergone an IP injection of NaF (0.5 μl @ 1% v/v). Fig. 1F shows a baseline image of the native fluorescence from the GFP-ApoE that is expressed in nerve axons and neurosensory retina. The SLO focal plane has been positioned at the VRI, which shows retinal vasculature, contrasted against GFP fluorescence signal being returned from both adjacent nerve axons and Müller glia within the inner retina. The green fluorescent expression in the NFL, GCL, and IPL accentuates the retinal vasculature space, which appears dark against a green background (Fig. 1F). After injection, the vessels can be seen filling with NaF at 15 (Fig. 1G), 30 (Fig. 1H) and 70 (Fig. 1I) seconds. Eventually, the NaF signal overwhelms the signal from the GFP-ApoE and as this happens, instrument gain must be changed to avoid signal saturation. As a result of the change in instrument sensitivity the GFP-ApoE signal fades in the image sequence and thus only the vasculature is seen in the final image (Fig. 1I). The use of a fluorescent label to accentuate the vitreoretinal interface (GFP-ApoE) greatly aids in performing these experiments because it allows the proper focal plane to be identified prior to NaF injection. However, despite our success with obtaining this “traditional” angiography data we found this to be a rather challenging task to routinely perform, especially in wild type fish with no GFP-ApoE label to serve as an initial alignment landmark. The small size of the fish coupled with the complications of injecting, all while simultaneously trying to image, proved to be tedious and very difficult to successfully perform on a consistent basis. Imaging the *Tg(l-fabp:DBP-EGFP)* line, on the other hand, was very simple (Fig. 1J, see Supplemental Video 2) as no injection of contrast agent is required.

A comparison between retinal angiograms of *Tg(l-fabp:DBP-EGFP)* zebrafish (Fig. 1J) and mice (Fig. 1K, L) injected with NaF (10μl @ 1% v/v, images collected 4 min post-IP injection) show substantial differences in vascular anatomy. Differences between zebrafish and mammals, including primates, have been previously reported (Alvarez et al., 2007). The zebrafish retina (Fig. 1J) lacks the superficial and deep vascular plexus that are prominent within the retina in mice (Fig. 1K, L). The zebrafish retinal vasculature (Fig. 1J) is restricted to the basal surface of the retina at the vitreoretinal interface. Because of the absence of intraretinal branches near the optic nerve, the vasculature of the zebrafish retina is significantly less complicated and congested than those from a mouse retina (Table 2).

These anatomical differences make measuring and quantifying the signal magnitude of the extravascular space easier to perform and show that background levels in zebrafish are significantly lower than in mice (Table 2). Extravascular background in zebrafish is equivalent to the mouse superficial plexus but significantly lower (factor of 2) than the mouse deep vascular plexus. In theory, the lower background observed in zebrafish relative to mice should enhance the ability to discern and detect leakage from the retinal vessels in fish as compared to those in mice.

This difference in extravascular signal background between species likely originates from multiple known and some potentially still unknown sources. Examples that could potentially influence signal magnitude are: (1) Instrument gain - the SLO sensitivity setting can alter the measured signal magnitude(Charbel Issa et al., 2012), (2) Pupil size – smaller fish are observed to have smaller pupils which act as an aperture and reduce illumination and signal collection efficiency as demonstrated in mice if not fully dilated (Charbel Issa et al., 2012), (3) Fluorescent protein expression and/or labeling – variances in expression of GFP among individual animals could influence signal (Duval et al., 2013), (4) Endogenous autofluorescence- lipofuscin in the mouse RPE, which accumulates with age, is a strong contributor to background signal when imaging in AF mode (Sparrow et al., 2013) whereas in contrast, the rod OS and RPE in light adapted zebrafish are shielded by melansomes (Hodel et al., 2006) and the retina in our experience, qualitatively do not fluoresce in a similar manner and intensity as mouse RPE, (5) Ocular opacity- media opacities are known to quickly occur in anesthetized mice (Ridder et al., 2002), and have been reported in some zebrafish models (Tschopp et al., 2010); these can contribute to light scattering and alter signal measurements, and finally (6) Stray signal collection from regions outside the SLO focus – A stacked (i.e. from superficial, intermediate and deep vascular plexus regions) vascular plexus in the mouse (Paques et al., 2006) could cause signal collection overlap between measurements from each individual layer. Fluorescence signal bleeding through from intermediate and deep levels will influence measurements of avascular signal from the superficial plexus and vice versa, measurements of avascular signal from the deep plexus will be influenced by signal being collected that is before and/or after this layer, namely from the superficial and intermediate vessels. One must be cognizant of the fact that the confocal region of signal collection (i.e. region of confocality) is not a finitely confined plane within the tissue. Instead it is a three-dimensional, semi-finite geometry with both a diameter (x-y plane) and axial length (z-axis plane) signal collection zone that is dependent on various optical parameters. These parameters can include both the optical system design within the SLO (e.g. pinhole size) and the ocular characteristics of the species being imaged (e.g. ocular refractive power, pupil diameter, etc.)(Delori et al., 2011). In general, the smaller the pinhole the more confined the sample collection region and the more discrimination there will be against collecting indirect scattered light (Woon et al., 1992). The HRA2 has a pinhole that is 300–400 μm and is designed for use in the human eye (Maass et al., 2007). Regardless of the size, every pinhole permits some amount of signal to be collected from objects before and after the optimal plane of focus if that signal is overwhelming. This can be observed in Fig. 1L which shows image artifact as a result of the signal originating from objects (i.e. large primary vessels) outside the region of optimal focus. In this image, the instrument focus has been positioned for viewing of the mouse deep

vascular plexus. Stray light is still being collected from the large vessels, which are very bright due to the volume of GFP reporter contained within the vascular compartment. The vessels, which are located in front of the plane of focus, still contribute signal since one must image through the superficial plane to collect information from the deep plexus. This is why these vessels lack clear definition, as they are located outside the plane of focus. To our knowledge, no one has measured, calculated or modeled how the rodent and zebrafish eye influences the parameters (e.g. degree of confocality, axial and lateral resolutions, confocal region axial and lateral geometry and/or size, etc.) of this particular instrument that has specifications designed and reported for the human eye. This information, if obtained would be most helpful to many research labs that are heavily using these instruments to study numerous animal models. One group, however, has performed some system alterations so that their SLO it is better optimized for mice (Sparrow et al., 2013) and perhaps this could also be done specifically for zebrafish as well to further improve system performance.

Tg(l-fabp:DBP-EGFP) zebrafish, which express endogenously-fluorescent, circulating EGFP contrast agent, have been previously employed for studying vascular leakage (Xie et al., 2010). Here we demonstrate how this model, used in conjunction with an SLO, can be used to study and quantify vascular leakage induction after intraocular injections of biological proteins or protein peptides. Fig.2 shows the results from an experiment where we purposely injected NaF mixed with BSA (NaF + BSA) to induce a simulated vascular leakage episode. The purpose of this experiment was three-fold. First, we needed to inject a positive control (i.e. fluorescent agent) into the eye that we could validate our quantitative analysis methods developed for this model. Second, since our injection technique is performed by hand, we wanted to get some idea of our injection success rate. Third, we wanted to demonstrate that one could use a fluorophore, such as NaF, ICG or others mixed with the desired test agent being delivered to provide immediate, post-injection feedback on the success of the injection attempt.

Baseline (BL) images were collected on the first day from each animal. On the following day, animals were anesthetized and injected with NaF+BSA. Immediately post-injection (IPI), animals were briefly recovered for a few minutes (~3 min) and then re-anesthetized for imaging. Thereafter, the animals were imaged again at 1, 2 and 4 days post-injection (DPI). Three sets of images (Figs. 2A–O) from 3 different zebrafish injected with NaF+BSA represent our observations. The results from this experiment are shown graphically in Fig. 2P. At BL, all zebrafish exhibited an ESMI that was ~15±10 grayscale units. Immediately after injection of NaF+BSA, the ESMI signal increased from between 2 (min) to 55-fold (max). On average, this change was significant (P=0.0185, Ordinary One-way ANOVA with Dunnett's Multiple Comparisons Test and adjusted P-value) relative to BL. Fig. 2A–E shows one animal that had the smallest change (2-fold) relative to the BL. IPI it can be seen that no increase in ESMI was documented (Fig. 2B), which essentially indicates that this particular injection was unsuccessful and no NaF was delivered. Figs. 2F–J demonstrates a typical (i.e. 5 of 8 injected that were similar in response) IOI observed during this experiment which clearly shows a change in avascular space appearance and signal intensity relative to the adjacent retinal vasculature. This result represents a 5.5-fold increase in ESMI over that observed at BL. Figs. 2K–O shows an injection that was highly successful in delivering a

large bolus of NaF+BSA. In this example, the ESMI increased an astounding 55-fold and this appears to represent a “direct hit” into the vitreous chamber. In other cases it was obvious that the injection was subretinal as IPI imaging showed vascular plexus deformation caused by the injected fluid bleb (image not shown). IPI (Fig. 2L) it can be observed that the NaF signal originating from the extravascular space is brighter that the EGFP circulating in the retinal vessels. Only one day later the NaF has cleared from the posterior chamber as the elevated ESMI levels observed IPI have returned to near-BL levels.

In Fig. 2P the dotted line represents the limit for a grayscale level of 251 units which indicates the point at which detection saturation occurs with the HRA2. Data points beyond this line are extrapolated using the correction methods detailed in 2.3.3. This experiment has clearly demonstrated that our injections are successful the majority of times but also reveals that the bolus being delivered is variable in delivery location (IVT, subretinal, intraretinal or fails completely) from one animal to another. From these examples one can easily conclude that adding a small amount of fluorophore to the injection bolus serves as a helpful indictor for determining IOI success. Absence of dye would indicate that the injection was unsuccessful and that this animal could be eliminated from further experimental analysis consideration. Furthermore, we were able to see vessel deformation after some injections that we believe are from subretinal blebs. Thus, it appears as if this imaging method can distinguish between subretinal and intravitreal injections. The dye that would be the best candidate for this purpose would be ICG or alternatively, other dyes that have excitation and emission ranges that overlap with the ICGA channel of the HRA2. IR fluorophores of this nature would be better to use than NaF as it would not interfere with the EGFP signal already present in *Tg(l-fabp:DBP-EGFP)* zebrafish.

In a second experiment we aimed to determine whether intraocular injections with a benign protein could cause vascular leakage in *Tg(l-fabp:DBP-EGFP)*. Results from this group were compared to another group of control animals conducted separately. In the control group, animals did not receive IOI but still underwent imaging at the second time point one day after BL images were collected (i.e. IPI). Representative examples of non-injected and BSA injected eyes are shown in Figs. 3A–E and Figs. 3F–J, respectively. In the non-injected control, no significant changes in ESMI were observed after repeated imaging sessions (Figs 3A–E). In contrast, the group injected with BSA shows a significant increase at 1 DPI {$P \leq 0.0001$ relative to baseline (Ordinary One-way ANOVA with Dunnett's Multiple Comparisons Test and adjusted P-value) and $P \leq 0.0001$ relative to non-injected controls at 1 DPI (Multiple t tests with significance determined by the Holm-Sidak method and 5% alpha)}. A visual example of this increase can be seen in Fig 2H, which makes the avascular space appear hazy relative to the baseline image (Fig. 3F). This observation persists through 2 DPI, and occasionally 4 DPI, but was found to be insignificant relative to baseline. This experiment demonstrates that injection of a benign protein can induce a significant change in ESMI relative to BL. At this point it is unclear whether this leakage represents EGFP-albumin leakage or if the injection has simply altered the background signal originating from the retina via some yet undocumented organ and/or tissue response (i.e. edema). Important to note is that no evidence of EGFP-albumin leakage occurred IPI on Day 2. The lack of an acute response suggests that the intraocular injection itself is not inducing EGFP leakage due

to vascular trauma (e.g. vessel rupture). Nevertheless, one must cognizant that injection trauma is a possibility at any time and could potentially influence experimental outcomes should it happen.

Fig 4 ultimately demonstrates the utility of applying SLO imaging to investigate vascular leakage in *Tg(l-fabp:DBP-EGFP)*. In this experiment we tested a protein peptide known to induce vascular permeability compared to a separate group of BSA injected animals. Figs. 4A–P show a panel of images that provide an example of the results observed with this experiment. Figs 4A–D, 4E–H, 4I–L & 4M–P are representative image examples from animals that received 20 ng of BSA or 20, 40 and 80 ng of BDK, respectively. BSA shows a moderate, but insignificant change in ESMI at 1 DPI relative to BL. There was one unusual outlier in the BSA treatment group (Fig. 4Q) this time that had an abnormally high response at 1 DPI (51.4 mean signal units @ 1 DPI vs. 14.6 units @ BL).

In the animals that received BDK we observed increased ESMI in each treatment group. Representative image examples from the 20, 40 and 80 ng treatment groups can be seen in Figs. 4E–H, 4I–L & 4M–P, respectively. The graphical representation of these results (Fig. 4Q) shows that both 20 & 40 ng doses exhibited similar results at 1 DPI. The ESMI increased by 6.5-fold (up ~100 from ~15 @ BL) with both doses. Easily observed from the graphical data (Fig. 4Q) is the delineation between responding and non-responding animals. In the 20 & 40 ng treatment groups, 3/4$^{th's}$ and 2/3^{rd,s} of animals, respectively, responded by showing obvious increases in ESMI. The ESMI of responders were clustered around 100 grayscale units vs. virtually no amplitude change for non-responders relative to BL.

At doses of 20 (Figs. 4E–H) & 40 ng (Figs. 4I–L), a significant increase ($P \leq 0.0001$; Two-way ANOVA with Dunnet's Multiple Comparisons Test) in ESMI was observed at 1 DPI. These elevated changes persist for another 24 hrs (2 DPI) but were fully resolved by 4 DPI. At 2 DPI, only the 20 ng treatment group was significant ($P=0.0061$). The group receiving 80 ng BDK showed some evidence of leakage (Fig. 4N) but the mean difference (+21 mean grayscale units) over the BSA group was found to be insignificant. By 2 DPI, all animals in the 80 ng BDK group had returned to values similar to those observed at BL and with BSA controls at 2 DPI.

3.5 Post-Imaging Care

The contact lens is removed immediately post-imaging. The fish are then transferred to a small weigh boat filled with tank water, positioned on a tared microbalance, and weighed. Upon return to the tank, the fish was monitored visually for operculum movement. If operculum movement is suppressed or delayed, water is expelled across its gills using a disposable plastic pipette to expedite recovery.

The contact lens should be cleaned with water so that residual index matching fluid or contaminants will be removed in preparation for the next animal. As described in section 3.3 above.

4.0 Potential Pitfalls and Troubleshooting

Our group is able to successfully image the retinal vasculature of adult zebrafish on a routine basis using SLO. A method for successfully preparing, imaging and recovering fish, for either single or multiple imaging sessions is now routine. We experienced low mortality rates (3%) in a substantial cohort of fish (n=34). We discovered that imaging procedures involving fish are quite easy to perform relative to other popular small animal models like mice for the following reasons: (1) mydriatics are not required, (2) anesthesia is less complicated, (3) ocular clarity remained stable (i.e. no cataract or ocular opacities develop) throughout the duration of the imaging period, and (4) less time is required to complete the imaging. Despite these advantages, fish are still somewhat challenging because they: (1) have very small pupils and thus require more skill and dexterity to properly positioning the instruments in order to acquire images and (2) require an aqueous environment for survival and thus can only be kept out of water for a small amount of time (no more than 10 minutes maximum).

Finally, several key issues are important when attempting to image zebrafish:

4.1 Animal preparation

As with any animal, the proper anesthesia level is critical. A systematic approach is best for establishing and refining a routine. Keep track of successes and failures and correlate them to anesthesia dose and experiment durations for anesthesia induction, imaging session and recovery times. For novices it is helpful to have one or more people responsible for fish anesthesia, preparation and documentation while a second individual is performing the imaging.

4.2 Contact Lens Type, Placement and Care

Imaging the native fish eye without aid from a contact lens produced poor results (images not shown). In contrast, use of a periorbital-affixed contact lens was overwhelmingly successful and provided informative images of retinal morphology. Several different contact lenses were tested in an attempt to qualitatively determine which would perform the best. Thin and/or small lenses were more difficult to handle, hard to visualize and susceptible to being displaced from the animal if the anesthesia was inadequate. Under these circumstances a larger lens (5 vs. ~3 mm diameter) was easier to locate after being thrown off by an under-anesthetized fish and handled on a regular basis for placement and removal. To accomplish successful imaging in fish it was not mandatory for the contact lens to be in direct contact and/or conforming to corneal surface. However, it was critically important to use a viscous or semi-viscous index matching fluid to (1) promote adhesion of the contact lens to the fish, and (2) eliminate the air bubbles from the space between the concave and convex surfaces of the contact lens and cornea, respectively. Our preferred fluid was Systane® Ultra, which permitted easy rinsing and cleaning of the lenses between imaging sessions. It was not critically important to have the contact lens perfectly centered over the eye. Often, the lens would be slightly off-center either in the caudal or nasal direction, but informative images could still be obtained. However, under this circumstance, one region of the retina would often have slightly better image quality than the other depending on which direction the

contact lens had shifted. Positioning asymmetry was easily addressed by manually repositioning the contact lens. This same approach was also performed when secondary, ghost images were observed of the retinal vasculature. Air bubbles in the index matching media or contaminants on the contact lens surface will cause duplication of detail (i.e. ghosting) in the images. In this case, a slight push or rotation of the contact lens would often rectify the problem. If this does not work then it was necessary to remove the lens, return the fish to its native environment, and clean the lens using a cotton-tipped applicator and clean water. Between daily imaging sessions the contact lens was disinfected using contact lens cleaning solution (Boston Simplus, Bausch & Lomb, Inc., Rochester, NY). Lens integrity and cleanliness was regularly inspected using a stereomicroscope (MZ9.5, Leica Microsystems, Buffalo Grove, IL) and cleaning was performed as needed. We have been using the same contact lenses (2 ea.) for several months involving more than several hundred individual fish imaging sessions. We have observed that the lens surfaces do become scratched over time due to handling with metal forceps but this does not seem to dramatically hinder image quality. At this time they appear to be capable of working indefinitely provided they are handled carefully and cleaned as aforementioned. Obviously, one will need to replace them at some point and take into consideration whether extended use may influence sensitive experiments involving quantitative measurements.

4.3 Animal Positioning

Positioning the fish quickly and efficiently is important. The SLIK model SBH-320 ball camera mount is invaluable for being able to position fish at the proper angle relative to the scanning SLO beam. Smaller fish are generally more difficult to image as clear access through the pupil is more challenging. Having a wide range in positioning freedom is advantageous. However, important to note is that it is not necessary to incorporate precise positioning mechanisms (i.e. micrometer actuated translation stages or positioning devices) to set up the fish for imaging. A crude mechanism, like the manually operated SBH-320 mount, is ideal since it is quick at positioning the fish in the approximate location. Afterwards the precise, three dimensional (X, Y, Z) positioning capabilities within the SLO can be used to carefully and rapidly align the instrument with the eye and ocular features of interest.

4.4 User Proficiency and Experience

With all techniques and methods, practice improves data quality and can impact experimental outcomes. Multiple imaging sessions greatly improve one's ability to collect high quality images. Investigators just beginning to use this imaging technology on zebrafish should not start with valuable experimental specimens. It takes some time to acquire the skills required to perform the eye-hand coordination that will yield the best quality images, but this is quickly achieved with practice.

Supplementary Material

Refer to Web version on PubMed Central for supplementary material.

Acknowledgements

The authors thank Didier Stainier and Ramani Ramchandran for providing *Tg(flk1:EGFP)* and *Tg(flk1:nGFP)* lines and Francesca Peri and Christiane Nusslein-Volhard for providing *Tg(apoeb:lynEGFP)zf147*. We also thank Walter Burgess from Heidelberg Engineering, Inc. for technical assistance. The study was supported in part by National Institutes of Health Grants R01-EY014240, R01-EY020861, K08-EY023608, an unrestricted grant from Research to Prevent Blindness, a Foundation Fighting Blindness Research Center Grant, The Wolf Family Foundation, the Llura and Gordon Gund Foundation, and the Cleveland Clinic.

Abbreviations

AF	Autofluorescence
YAT	Yen Auto-Threshold
ESMI	Extravascular Space Mean Intensity
ESMA	Extravascular Space Mean Area
BL	Baseline
BSA	Bovine Serum Albumin
BDK	Bradykinin
CNV	Choroidal Neovascularization
CFM	Confocal microscopy
DPI	Days Post-Injection
D	Diopter
EGFP	Enhanced Green Fluorescent Protein
FOV	Field of view
GCL	Ganglion cell layer
GFP	Green fluorescent protein
HRA2	Heidelberg Retina Angiograph 2
IPI	Immediate Post-Injection
ICG	Indocyanine Green
ICGA	Indocyanine Green Angiography
IRAF	Infrared Autofluorescence
IRDF	Infrared-Dark Field
IR	Infrared Reflectance
IPL	Inner Plexiform Layer
IOI	Intraocular Injection
IVI	Intravitreal Injection
MP	Megapixel

NFL	Nerve Fiber Layer
OCT	Optical Coherence Tomography
RFP	Red Fluorescent Protein
RFDF	Red Free-Dark Field
ROI	Region of Interest
SLO	Scanning Laser Ophthalmoscopy/Ophthalmoscope
NaF	Sodium Fluorescein
FA	Sodium Fluorescein Angiography
VRI	Vitreoretinal Interface

References

Alvarez Y, Cederlund ML, Cottell DC, Bill BR, Ekker SC, Torres-Vazquez J, Weinstein BM, Hyde DR, Vihtelic TS, Kennedy BN. Genetic determinants of hyaloid and retinal vasculature in zebrafish. Bmc Dev Biol. 2007; 7:114. [PubMed: 17937808]

Bailey TJ, Davis DH, Vance JE, Hyde DR. Spectral-domain optical coherence tomography as a noninvasive method to assess damaged and regenerating adult zebrafish retinas. Investigative ophthalmology & visual science. 2012; 53:3126–3138. [PubMed: 22499984]

Balaggan KS, Binley K, Esapa M, MacLaren RE, Iqball S, Duran Y, Pearson RA, Kan O, Barker SE, Smith AJ, Bainbridge JW, Naylor S, Ali RR. EIAV vector-mediated delivery of endostatin or angiostatin inhibits angiogenesis and vascular hyperpermeability in experimental CNV. Gene Ther. 2006; 13:1153–1165. [PubMed: 16572190]

Beck SC, Schaeferhoff K, Michalakis S, Fischer MD, Huber G, Rieger N, Riess O, Wissinger B, Biel M, Bonin M, Seeliger MW, Tanimoto N. In vivo analysis of cone survival in mice. Investigative ophthalmology & visual science. 2010; 51:493–497. [PubMed: 19737879]

Bilotta J, Saszik S. The zebrafish as a model visual system. Int J Dev Neurosci. 2001; 19:621–629. [PubMed: 11705666]

Charbel Issa P, Singh MS, Lipinski DM, Chong NV, Delori FC, Barnard AR, MacLaren RE. Optimization of in vivo confocal autofluorescence imaging of the ocular fundus in mice and its application to models of human retinal degeneration. Invest Ophthalmol Vis Sci. 2012; 53:1066–1075. [PubMed: 22169101]

Dahm R, Schonthaler HB, Soehn AS, van Marle J, Vrensen GF. Development and adult morphology of the eye lens in the zebrafish. Experimental eye research. 2007; 85:74–89. [PubMed: 17467692]

Delori F, Greenberg JP, Woods RL, Fischer J, Duncker T, Sparrow J, Smith RT. Quantitative measurements of autofluorescence with the scanning laser ophthalmoscope. Investigative ophthalmology & visual science. 2011; 52:9379–9390. [PubMed: 22016060]

Duval MG, Chung H, Lehmann OJ, Allison WT. Longitudinal fluorescent observation of retinal degeneration and regeneration in zebrafish using fundus lens imaging. Mol Vis. 2013; 19:1082–1095. [PubMed: 23734077]

Farkas DL, Cheng Y-H, Yu J-Y, Wu H-H, Huang B-J, Chu S-W, Nicolau DV, Leif RC. Spectral ophthalmoscopy based on supercontinuum. SPIE Proc. 2010; 7568:75680I–75685.

Hassenstein A, Meyer CH. Clinical use and research applications of Heidelberg retinal angiography and spectral-domain optical coherence tomography - a review. Clin Experiment Ophthalmol. 2009; 37:130–143. [PubMed: 19338610]

Heidelberg Engineering. 55° Wide Field Objective User Information (Art. No. 97 109-002) Heidelberg Retina Angiograph 2 Release Notes (Art. No. 11296). Heidelberg Engineering GmbH. 2006:1–7.

Heidelberg Engineering. Imaging the Retina of Mice, Spectralis HRA/HRA2 Mouse Kit. Heidelberg Engineering,GmbH. 2008:20941–20946. Art. NO. 20942.

Hodel C, Neuhauss SC, Biehlmaier O. Time course and development of light adaptation processes in the outer zebrafish retina. The anatomical record. Part A, Discoveries in molecular, cellular, and evolutionary biology. 2006; 288:653–662.

Hossain P, Liversidge J, Cree MJ, Manivannan A, Vieira P, Sharp PF, Brown GC, Forrester JV. In vivo cell tracking by scanning laser ophthalmoscopy: quantification of leukocyte kinetics. Investigative ophthalmology & visual science. 1998; 39:1879–1887. [PubMed: 9727411]

Howe K, Clark MD, Torroja CF, Torrance J, Berthelot C, Muffato M, Collins JE, Humphray S, McLaren K, Matthews L, McLaren S, Sealy I, Caccamo M, Churcher C, Scott C, Barrett JC, Koch R, Rauch G-J, White S, Chow W, Kilian B, Quintais LT, Guerra-Assuncao JA, Zhou Y, Gu Y, Yen J, Vogel J-H, Eyre T, Redmond S, Banerjee R, Chi J, Fu B, Langley E, Maguire SF, Laird GK, Lloyd D, Kenyon E, Donaldson S, Sehra H, Almeida-King J, Loveland J, Trevanion S, Jones M, Quail M, Willey D, Hunt A, Burton J, Sims S, McLay K, Plumb B, Davis J, Clee C, Oliver K, Clark R, Riddle C, Eliott D, Threadgold G, Harden G, Ware D, Mortimer B, Kerry G, Heath P, Phillimore B, Tracey A, Corby N, Dunn M, Johnson C, Wood J, Clark S, Pelan S, Griffiths G, Smith M, Glithero R, Howden P, Barker N, Stevens C, Harley J, Holt K, Panagiotidis G, Lovell J, Beasley H, Henderson C, Gordon D, Auger K, Wright D, Collins J, Raisen C, Dyer L, Leung K, Robertson L, Ambridge K, Leongamornlert D, McGuire S, Gilderthorp R, Griffiths C, Manthravadi D, Nichol S, Barker G, Whitehead S, Kay M, Brown J, Murnane C, Gray E, Humphries M, Sycamore N, Barker D, Saunders D, Wallis J, Babbage A, Hammond S, Mashreghi-Mohammadi M, Barr L, Martin S, Wray P, Ellington A, Matthews N, Ellwood M, Woodmansey R, Clark G, Cooper J, Tromans A, Grafham D, Skuce C, Pandian R, Andrews R, Harrison E, Kimberley A, Garnett J, Fosker N, Hall R, Garner P, Kelly D, Bird C, Palmer S, Gehring I, Berger A, Dooley CM, Ersan-Urun Z, Eser C, Geiger H, Geisler M, Karotki L, Kirn A, Konantz J, Konantz M, Oberlander M, Rudolph-Geiger S, Teucke M, Osoegawa K, Zhu B, Rapp A, Widaa S, Langford C, Yang F, Carter NP, Harrow J, Ning Z, Herrero J, Searle SMJ, Enright A, Geisler R, Plasterk RHA, Lee C, Westerfield M, de Jong PJ, Zon LI, Postlethwait JH, Nusslein-Volhard C, Hubbard TJP, Crollius HR, Rogers J, Stemple DL. The zebrafish reference genome sequence and its relationship to the human genome. Nature. 2013; 496:498–503. [PubMed: 23594743]

Hughes V. Will This Fish Transform Medicine? Popular Science. 2013

Jin SW, Beis D, Mitchell T, Chen JN, Stainier DY. Cellular and molecular analyses of vascular tube and lumen formation in zebrafish. Development. 2005; 132:5199–5209. [PubMed: 16251212]

Kagemann L, Ishikawa H, Zou J, Charukamnoetkanok P, Wollstein G, Townsend KA, Gabriele ML, Bahary N, Wei X, Fujimoto JG, Schuman JS. Repeated, noninvasive, high resolution spectral domain optical coherence tomography imaging of zebrafish embryos. Mol Vis. 2008; 14:2157–2170. [PubMed: 19052656]

Kari G, Rodeck U, Dicker AP. Zebrafish: an emerging model system for human disease and drug discovery. Clinical pharmacology and therapeutics. 2007; 82:70–80. [PubMed: 17495877]

Luhmann UF, Robbie S, Munro PM, Barker SE, Duran Y, Luong V, Fitzke FW, Bainbridge JW, Ali RR, MacLaren RE. The drusenlike phenotype in aging Ccl2-knockout mice is caused by an accelerated accumulation of swollen autofluorescent subretinal macrophages. Investigative ophthalmology & visual science. 2009; 50:5934–5943. [PubMed: 19578022]

Maass A, von Leithner PL, Luong V, Guo L, Salt TE, Fitzke FW, Cordeiro MF. Assessment of rat and mouse RGC apoptosis imaging in vivo with different scanning laser ophthalmoscopes. Current eye research. 2007; 32:851–861. [PubMed: 17963105]

Matthews M, Varga ZM. Anesthesia and Euthanasia in Zebrafish. Ilar Journal. 2012; 53:192–204. [PubMed: 23382350]

McLellan GJ, Rasmussen CA. Optical coherence tomography for the evaluation of retinal and optic nerve morphology in animal subjects: practical considerations. Veterinary Ophthalmology. 2012; 15:13–28. [PubMed: 22805095]

Paques M, Simonutti M, Roux MJ, Picaud S, Levavasseur E, Bellman C, Sahel JA. High resolution fundus imaging by confocal scanning laser ophthalmoscopy in the mouse. Vision research. 2006; 46:1336–1345. [PubMed: 16289196]

Peri F, Nusslein-Volhard C. Live imaging of neuronal degradation by microglia reveals a role for v0-ATPase a1 in phagosomal fusion in vivo. Cell. 2008; 133:916–927. [PubMed: 18510934]

Podoleanu A, Verma Y, Divakar Rao K, Gupta PK. In-vivo imaging of adult zebrafish using optical coherence tomography. SPIE Proc. 2008; 7139:71390H–71396.

Rao KD, Verma Y, Patel HS, Gupta PK. Non-invasive ophthalmic imaging of adult zebrafish eye using optical coherence tomography. Current Science. 2006; 90:1506–1510.

Rasband, WS. ImageJ. U. S. National Institutes of Health; Bethesda, Maryland, USA: 1997–2012. http://imagej.nih.gov/ij/

Ridder W III, Nusinowitz S, Heckenlively JR. Causes of cataract development in anesthetized mice. Experimental eye research. 2002; 75:365–370. [PubMed: 12384099]

Seeliger MW, Beck SC, Pereyra-Munoz N, Dangel S, Tsai JY, Luhmann UF, van de Pavert SA, Wijnholds J, Samardzija M, Wenzel A, Zrenner E, Narfstrom K, Fahl E, Tanimoto N, Acar N, Tonagel F. In vivo confocal imaging of the retina in animal models using scanning laser ophthalmoscopy. Vision research. 2005; 45:3512–3519. [PubMed: 16188288]

Sparrow JR, Blonska A, Flynn E, Duncker T, Greenberg JP, Secondi R, Ueda K, Delori FC. Quantitative fundus autofluorescence in mice: correlation with HPLC quantitation of RPE lipofuscin and measurement of retina outer nuclear layer thickness. Investigative ophthalmology & visual science. 2013; 54:2812–2820. [PubMed: 23548623]

Tschopp M, Takamiya M, Cerveny KL, Gestri G, Biehlmaier O, Wilson SW, Strahle U, Neuhauss SCF. Funduscopy in Adult Zebrafish and Its Application to Isolate Mutant Strains with Ocular Defects. PloS one. 2010; 5

Vogel AM, Weinstein BM. Studying vascular development in the zebrafish. Trends in cardiovascular medicine. 2000; 10:352–360. [PubMed: 11369262]

Watanabe K, Nishimura Y, Oka T, Nomoto T, Kon T, Shintou T, Hirano M, Shimada Y, Umemoto N, Kuroyanagi J, Wang ZP, Zhang Z, Nishimura N, Miyazaki T, Imamura T, Tanaka T. In vivo imaging of zebrafish retinal cells using fluorescent coumarin derivatives. Bmc Neuroscience. 2010; 11

Webb RH, Hughes GW, Delori FC. Confocal scanning laser ophthalmoscope. Appl Opt. 1987; 26:1492–1499. [PubMed: 20454349]

Weinstein BM, Stemple DL, Driever W, Fishman MC. Gridlock, a localized heritable vascular patterning defect in the zebrafish. Nat Med. 1995; 1:1143–1147. [PubMed: 7584985]

Westerfield, M. The Zebrafish Book. 5th ed. University of Oregon Press; Eugene, Oregon: 2007.

Woon WH, Fitzke FW, Bird AC, Marshall J. Confocal imaging of the fundus using a scanning laser ophthalmoscope. The British journal of ophthalmology. 1992; 76:470–474. [PubMed: 1390528]

Xia CH, Liu H, Cheung D, Wang M, Cheng C, Du X, Chang B, Beutler B, Gong X. A model for familial exudative vitreoretinopathy caused by LPR5 mutations. Hum Mol Genet. 2008; 17:1605–1612. [PubMed: 18263894]

Xie J, Farage E, Sugimoto M, Anand-Apte B. A novel transgenic zebrafish model for blood-brain and blood-retinal barrier development. Bmc Dev Biol. 2010; 10

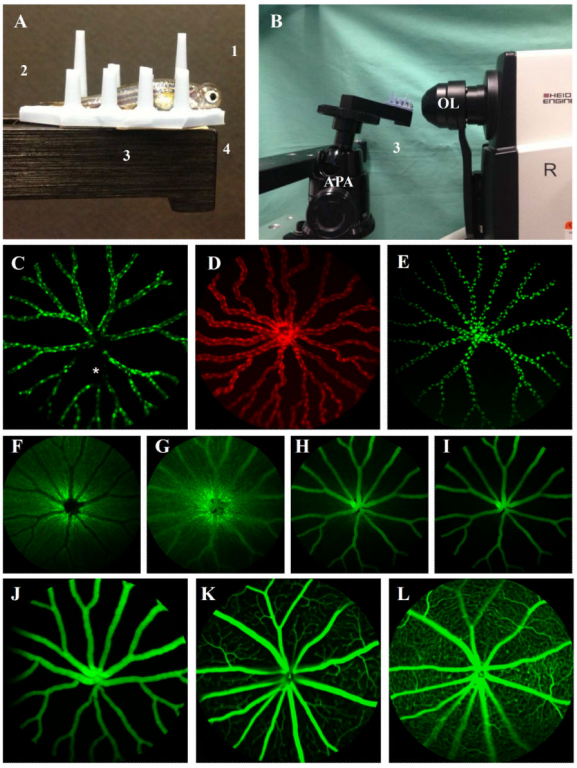

Figure 1.

Photographs of the experimental setup used to perform SLO of adult zebrafish (Fig. 1A,B) and representative images from zebrafish (Fig. 1C–J) compared to mice (Fig. 1K, L). Fig. 1A shows a fish prepared for imaging with a 5.2mm (Ø) PMMA contact lens (1) over the right eye. The fish is held upright between posts on the silicone finger mat (2). The mat also serves as a transportation aid to take the fish from the site of preimaging preparation (i.e. where the contact lens is applied) to the imaging instrument. The mat is placed on the positioning platform (3) and affixed to it using double-side tape (4). Scale bar = 1 cm. Fig. 1B shows the fish in position directly in front of the objective lens (OL) for imaging the right eye. The setup includes an alignment positioning apparatus (APA) and positioning platform (3) for quickly orienting the animal and eye for image collection. SLO images (pseudo-colored green or red depending on fluorescent protein emission wavelength maxima) from *Tg(flk1:EGFP)*(Fig. 1C), *Tg(flk1:mCherry)*(Fig. 1D), *Tg(flk1:nGFP)*(Fig. 1E), *Tg(apoeb:lynEGFP)zf147* (Fig. 1F) and *Tg(l-fabp:DBP-EGFP)*(Fig. 1J) zebrafish show fluorescent protein expression of endothelial cell cytoplasm and nuclei, glia and DBP (albumin), respectively. In Fig 1C, some EGFP expression signal dropout can be seen (asterisk) which we occasionally observed in both endothelial nuclei and cytoplasm lines. Switching the instrument to IR mode and visualizing the vessels with this channel confirmed that the vasculature was still intact and functional (not shown). Angiography of a *Tg(apoeb:lynEGFP)zf147* zebrafish (Fig. 1F–I) showing rapid filling of retinal vessels at 15 (Fig. 1G), 30 (Fig. 1H) and 70 (Fig. 1I) seconds post IP injection of 1% NaF. A comparison between fluorescent images from *Tg(l-fabp:DBP-EGFP)*(Fig. 1J) zebrafish and mouse (Fig. 1K–L) demonstrate the anatomical differences observed between species. Fig. 1K and 1L are FA images from the superficial and deep vascular plexus, respectively, from a normal

wild type mouse shown for comparison to a zebrafish in which the plexus are nonexistent (Fig. 1J). The zebrafish avascular space is much less congested than the mouse since they lack numerous capillary and venule branching from primary and secondary vessels emerging for the optic nerve. This simplifies quantitative analysis, as less rigorous algorithms are required for segmentation of vascular and avascular regions. Theoretically, less congestion should also contribute to a lower avascular signal background for which to visualize and detect leakage.

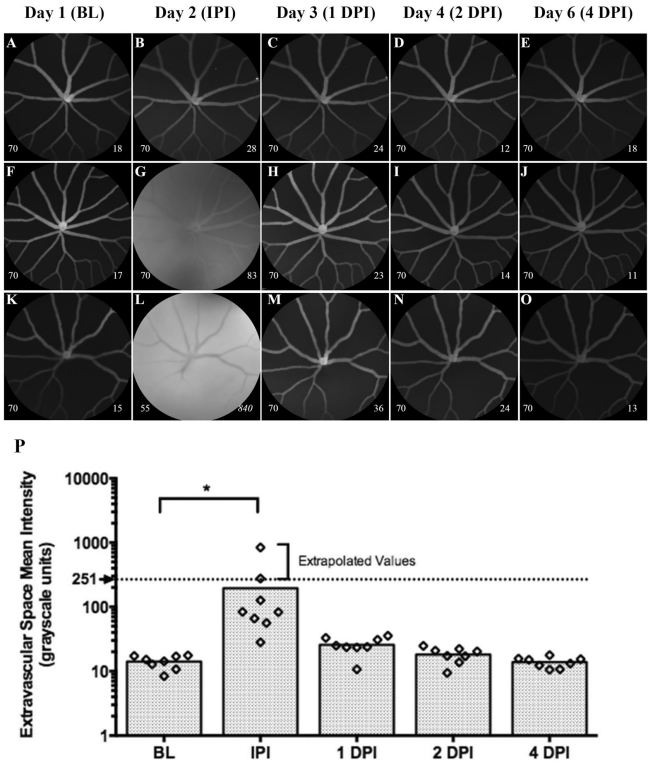

Figure 2.

Representative images (Fig. 2A–O) and graphical results (Fig. 2P) from an experiment conducted to demonstrate the data collection and quantitative analysis methods developed for detecting vascular leakage in *Tg(l-fabp:DBP-EGFP)*. In this group of animals (n=8), an intraocular injection of NaF+BSA (20ng, 0.8μl) was administered 1 day after BL imaging. Each animal was imaged immediately post-injection (IPI) to survey for the presence of NaF signal and then followed for 1, 2 & 4 days post-injection (DPI). Numbers on the lower left and right corners of each image represent the HRA2 camera sensitivity setting and the ESMI for that image, respectively. ESMI values that are italicized have been corrected using the methods outlined in Sec. 2.3.3. Figs. 2B, 2G, & 2L show examples of an unsuccessful, typical and highly successful IOI. IPI, NaF signal was observed in 7 out of 8 animals injected (88% success rate), however, the amount delivered was variable as we documented a 10-fold difference between minimum and maximum NaF signal magnitudes in typical (Fig. 2G) vs. highly (Fig. 2L) successful animals, respectively. The dotted line demarcates 251 gray levels and the maximum intensity value that can be directly measured with the HRA2 8-bit camera photodetection system. Mean values shown above this line have been extrapolated using the correction methods detailed in Section 2.3.3. Note that NaF signal is not retained for long as it is completely cleared within 24 hrs. Data shown as a scatter plot with bars to indicate group time point means.

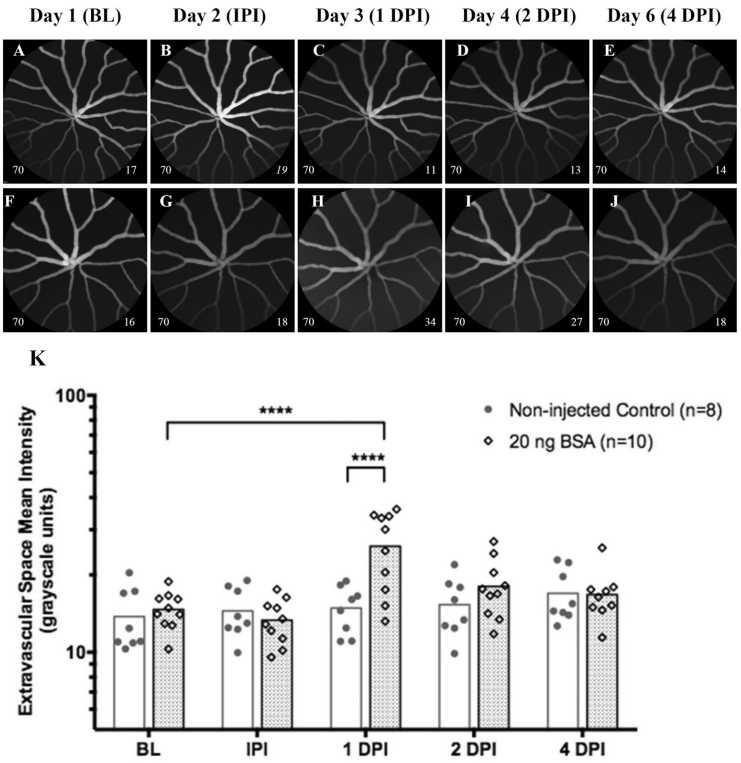

Figure 3.

Representative images (Fig. 3A–J) and graphical results (Fig. 3K) from an experiment involving IOI of BSA (20 ng, 0.8μl) in a group of *Tg(l-fabp:DBP-EGFP)* zebrafish compared to another group that did not receive injections. Fig. 3A–E and 3F–J show representative images collected from a non-injected and BSA-injected animal, respectively. Repeated imaging sessions in the injection-free group did not significantly change avascular space mean signal magnitude over time (Fig. 3K). In contrast, animals that received injections of BSA had a significant increase in mean signal magnitude at 1 DPI and can be observed in Fig. 3H as extravascular haze. This increase was significant relative to both the original mean baseline level on day 1, as well to the mean level observed at 1 DPI for the non-injected group. This response was brief and resolved within 24 hrs to an insignificant level at 2 DPI. Important to note is that no increase in ASMI was observed IPI, which demonstrates that the IOI does not cause acute damage resulting in leakage of EGFP-albumin. Data shown as a scatter plot with bars to indicate group time point means. (**Image notations: Lower left** # − camera sensitivity setting; **Lower Right** # - ESMI; **normal style text**- ESMI obtained with sensitivity set @ 70, ***italicized text***- ESMI was corrected).

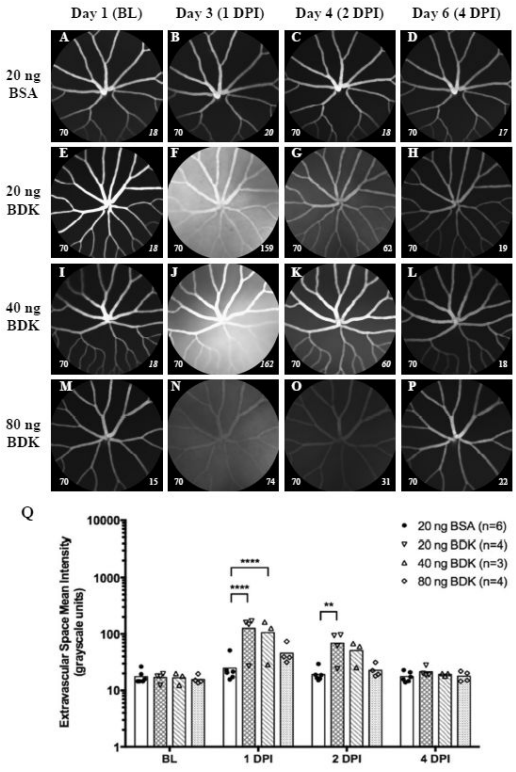

Figure 4.

Representative images (Fig. 4A–P) and graphical results (Fig. 3Q) from an experiment involving intraocular injections of BSA (20 ng, 0.8μl) as a control protein and BDK (20, 40 or 80ng, 0.8μl) in *Tg(l-fabp:DBP-EGFP)* zebrafish. Representative images from 20ng BSA and 20, 40 & 80ng of BDK can be observed in Figs. 4A–D, 4E–H, and 4I–L, respectively. One animal in the 40ng group died after baseline imaging. In this particular group of BSA treated animals (vs. the ones from Fig. 3), ASMI at 1 DPI was elevated relative to BL but not significant. Animals treated with BDK showed a significant response to treatment that could be easily observed at 1 DPI and moreover, the response carried over to 2 DPI. Leakage was observed in each treatment group but was significant only with 20 & 40 ng doses. This data also suggests an inverse dose response trend with BDK. This experiment shows the utility of this approach for the testing and screening of biological and chemical agents to study vascular permeability of the blood- retinal barrier. Data shown as a scatter plot with bars to indicate group time point means. (**Image notations: Lower left** # − camera sensitivity setting; **Lower Right** # - ESMI; **normal style text**- ESMI obtained with sensitivity set @ 70, ***italicized text***- ESMI was corrected).

Table 1

Characteristics of HRA2 SLO reflectance and angiography operating modes and sub-modes.

Reflection Mode (Dark field)				
Mode Channels	**Channel (abbrev.)**	**Laser Illumination Wavelength (nm)**	**Reflected Wavelength Collection (nm)**	**Source of Reflected Signal**
Infrared	*IRDF*	*815*	*815*	*reflected/scattered light (altered by tissue birefringence)*
Red Free*	*RFDF*	*488*	*488*	

Angiography Mode				
Mode Channels	**Channel (abbrev.)**	**Laser Excitation Wavelength (nm)**	**Emission Collection Range (nm)**	**Source of Emission Signal**
Sodium Fluorescein	*FA*	*488*	*500–680*	*NaF fluorescence or native autofluorescence*
Indocyanine Green	*ICGA*	*790*	*>800*	*ICG fluorescence or native autofluorescence*
Infrared†	*IR*	*815*	*815*	*reflected/scattered light*

* Red Free channel does not operate as a true dark field channel when used with the 55° Wide-field objective lens since the 488nm laser excitation beam emerging from the instrument is not 100% linearly polarized.

† Infrared channel is not used as an angiography channel but falls into this category because of instrument design. This is an “open” channel that lacks any optical filtering to eliminate the illumination laser wavelength @ 815nm. Light collected with this channel is autoreflected from ocular tissue constituents.

Table 2

A comparison between GFP and NaF angiography in zebrafish vs. mice. Mouse data was obtained from images collected at 4 min post- IP injection with 1% NaF. Zebrafish have more extravascular area for which to measure changes in extravascular leakage. Imaging system sensitivity (i.e. camera gain setting) was not significantly different between imaging groups and thus did not influence either extravascular area or intensity measurement comparisons. Data shown as Mean ± S.D and analyzed using an Ordinary one-way ANOVA with Dunnet's Multiple Comparisons Test.

SLO Image Characteristics	Zebrafish (n=10)	Mouse (n=6)	
	superficial	superficial	deep
Extravascular Space Mean Area (%, range 0–100)	*80.7 ± 1.9*	*60.5 ± 8.2*****	*47.2 ± 92*****
Extravascular Space Mean Intensity (grayscale units, range 0–251)	*17.5 ± 8.9*	*23.8 ± 10.6*$^{n.s.}$	*35.3 ± 12.6***
Camera Sensitivity Setting (console dial setting, range 31–107)	*67.5 ± 2.1*	*67.2 ± 9.5*	*68 ± 7.8*